This article has been accepted for publication in IEEE Geoscience and Remote Sensing Letters. This is the author's version which has not been fully edited and content may change prior to final publication. Citation information: DOI 10.1109/LGRS.2025.3565808

Covariance Matrix Estimation via Geometric Median in Highly Heterogeneous PolSAR Images

Dehbia Hanis, Luca Pallotta, *Senior Member, IEEE*, Karima Hadj-Rabah, *Member, IEEE*, Azzedine Bouaraba, and Aichouche Belhadj-Aissa

***Abstract*—The Wishart distribution is a well-established statistical model for characterizing the density of random variables in Polarimetric SAR (PolSAR) data, particularly within homogeneous regions where Gaussian assumptions hold. However, as PolSAR applications expand into heterogeneous environments, alternative statistical models have been developed to better capture the complexity of such areas, playing an important role in tasks such as classification. In this study, we examine the effectiveness of covariance matrix estimation using the median matrix, a technique grounded in optimal transport theory and validated in prior research for its effectiveness. Building on this foundation, we propose the application of a statistical model tailored for heterogeneous regions, i.e., following the $\mathcal{G}_P^0$ distribution, addressing the limitations of traditional assumptions. This method is particularly suitable for high-resolution PolSAR datasets, where the homogeneity hypothesis often does not hold. The experimental results obtained using L-band PolSAR images acquired over Foulum in Denmark demonstrate the robustness of our proposed variant.**

***Index Terms*—covariance estimation, $\mathcal{G}_P^0$ distribution, heterogeneous PolSAR images, median matrix, unsupervised classification.**

I. Introduction

The statistical properties of Synthetic Aperture Radar (SAR) data are crucial in many Earth observation image processing applications. Hence, several studies have been conducted, and various distributions have been employed to characterize the complexity of SAR data [1]. Many of these distributions arise from the multiplicative model assumption, leading to univariate distributions such as Rayleigh, exponential, Gamma, square root of Gamma, and the class of $\mathcal{K}$ distributions. Another important class, the univariate $\mathcal{G}$ family, was specifically introduced to model highly heterogeneous areas, including urban regions and other complex targets [2], [3]. More precisely, for homogeneous targets, negative exponential and Rayleigh distributions are commonly used for single-look intensity and amplitude, while Gamma and square root Gamma distributions are applied for the multi-look case. If homogeneity assumption is not verified, $\mathcal{K}$ is one of the most widely used distributions. Moreover, Frery *et al.* [2] introduced a comprehensive class of statistical models denoted $\mathcal{G}$-distributions, developed to characterize radar backscatter data across varying levels of heterogeneity. A particular case of this class, the $\mathcal{G}^0$ model, demonstrated high effectiveness in representing single-channel SAR data, including intensity, amplitude, and complex formats. This distribution showed superior adaptability in modeling clutter within extremely heterogeneous environments such as urban, forested, and deforested areas, where $\mathcal{K}$-distributions fail. Its flexibility emerges from its two parameters, one of which relates to the degree of homogeneity, including scaled speckle as a limiting case.

Building upon the univariate $\mathcal{G}$ family, the multivariate $\mathcal{G}_P$ distribution was introduced to extend its applicability to polarimetric SAR (PolSAR) data. This generalization retains the structure of the classical multi-look polarimetric $\mathcal{K}_P$ distribution while offering enhanced modeling capabilities. Notably, $\mathcal{K}_P$ is a special case of $\mathcal{G}_P$, but a more expressive and flexible alternative is given by the $\mathcal{G}_P^0$ model. Empirical studies have demonstrated that $\mathcal{G}_P^0$ is particularly effective for representing highly heterogeneous clutter, outperforming classical models in urban areas, bare soil, and other complex scattering environments.

Several advancements have been made in exploiting $\mathcal{G}_P^0$-based models for PolSAR image analysis and classification [4]–[7]. For instance, Horta *et al.* [4] conducted a comparison of random and quantile-based initializations for the stochastic Expectation-Maximization (EM) algorithm using $\mathcal{G}_P^0$ mixtures for segmentation purposes. Moreover, in [5], a robust semi-supervised EM-based classification method for multilook PolSAR data modeled by $\mathcal{G}_P^0$ was presented. The authors in [7] focused on the $\mathcal{G}^0$-Wishart model's flexibility in representing regions of varying heterogeneity in multilook PolSAR images. To this end, they applied H/A/$\overline{\alpha}$ decomposition and Iterated Conditional Modes algorithms to achieve effective classification. Additionally, the $\mathcal{G}_P^0$ model has been applied to polarimetric data collected by two airborne SAR systems, demonstrating its capacity to model diverse target types and reinforce its versatility beyond classical models.

Empirical analyses on PolSAR data have demonstrated that the $\mathcal{G}_P^0$ distribution outperforms others in representing complex scattering phenomena, thereby laying the groundwork for advanced image modeling and parameter estimation in SAR applications. Therefore, this study aims to adopt the $\mathcal{G}_P^0$ distribution to improve the modeling of the multi-look polarimetric covariance matrix. More specifically, we propose a new estimator for the polarimetric covariance matrix, obtained

D. Hanis (*corresponding author*), and A. Belhadj-Aissa are with the laboratory of Image Processing and Radiation (LTIR), University of Sciences and Technology Houari Boumedienne (USTHB), Algiers, Algeria. E-mail: dehbia_hanis@yahoo.com, houria.belhadjaissa@gmail.com.

L. Pallotta is with Department of Engineering (DiING), University of Basilicata, via dell'Ateneo Lucano 10, 85100 Potenza, Italy. E-mail: luca.pallotta@unibas.it.

K. Hadj-Rabah is with Department of Geoinformatics Z GIS, Paris-Lodron University of Salzburg, Salzburg, Austria. E-mail: hadjrabah@hotmail.fr.

A. Bouaraba is with Radar Laboratory, Ecole Militaire Polytechnique, Algiers, Algeria. E-mail: azzedine.bouaraba.emp@gmail.com.

resorting to the geometric median of some basic covariance matrix estimates. More precisely, the median matrix is defined as that matrix minimizing the average sum of the distance from the elementary set. The effectiveness of the proposed method has been assessed on the L-band fully polarized EMISAR data. To summarize our contributions, innovations introduced by the proposed framework are outlined as follows:

1) Formulation of an optimization problem for polarimetric covariance matrix estimation that accounts for heterogeneity in the data, by exploiting the $\mathcal{G}_P^0$ distribution.
2) Derivation of an optimal solution to the resulting optimization problem, represented by the median matrix of elementary estimates from individual data points.
3) Comprehensive experiments conducted using real case scenarios from fully polarized SAR data.

II. Background

Modeling complex multi-look covariance matrices can be achieved using three multivariate distributions: Wishart, $\mathcal{K}$ and $\mathcal{G}^0$ for homogeneous, heterogeneous and extremely heterogeneous areas respectively [8]. These three models belong to the $\mathcal{G}$-family, which is a multiplicative model that relates the distribution of the data (modeled as a generalized inverse Gaussian), to that of the speckle (that is Wishart distributed, being it considered as random Gaussian). The above three models are derived from specific cases of the generalized inverse Gaussian distribution: the uniform distribution for homogeneous areas, the Gamma distribution for heterogeneous areas, and the reciprocal Gamma distribution for extremely heterogeneous areas. In [3] (under some technical assumptions), models for the complex multi-look polarimetric covariance matrix have been established for heterogeneous and extremely heterogeneous areas as special cases of the $\mathcal{G}_P^0$ distribution.

Let us consider the polarimetric scattering vector $\boldsymbol{k}$:

$$\boldsymbol{k} = [S_{HH}, S_{HV}, S_{VV}]^T. \tag{1}$$

The covariance matrix modeling the terrain backscatters, i.e., the second order moment, of the complex data $\boldsymbol{k}$, denoted as $\boldsymbol{C}$, can be defined as:

$$\boldsymbol{C} = \mathbb{E}[\boldsymbol{k}\boldsymbol{k}^H], \tag{2}$$

with $\mathbb{E}[\cdot]$ the statistical expectation. According to [3], the heterogeneous areas model of the complex multi-look covariance matrix, obtained assuming $\xi > 0$, i.e.:

$$f_{(n)}(\boldsymbol{Z}) = \frac{2|\boldsymbol{Z}|^{n-m}(n\xi)^{(\xi+nm)/2}}{h(n,m)|\boldsymbol{C}|^n\Gamma(\xi)} \left(\text{trace}\left(\boldsymbol{C}^{-1}\boldsymbol{Z}\right)\right)^{\frac{(\xi-nm)}{2}} K_\xi - nm\left(2\sqrt{n\xi\text{trace}\left(\boldsymbol{C}^{-1}\boldsymbol{Z}\right)}\right), \tag{3}$$

where $\boldsymbol{Z}$ is the complex n-looks sample covariance matrix (SCM) of the observables (e.g., terrain plus speckle noise), defined as follows:

$$\boldsymbol{Z} = \frac{1}{n}\sum_{i=1}^{n}\boldsymbol{k}_i\boldsymbol{k}_i^H. \tag{4}$$

Moreover, $\Gamma(\cdot)$ denotes the Gamma function, $K_\nu(\cdot)$ is the modified Bessel function of the third kind and order ν, and $m = 3$ is the polarimetric vector size. Finally, $h(n,m) = \pi^{m(m-1)/2}\Gamma(n)\cdots\Gamma(n-m+1)$.

Note that, the parameter ξ measures the roughness or the texture since it is related to the number of elementary backscatterers in the resolution cell [3] [9]. It is estimated as the mean of the three roughness parameters of each polarization ξ_{HH}, ξ_{HV} and ξ_{VV}:

$$\xi = \frac{\xi_{HH} + \xi_{HV} + \xi_{VV}}{3}. \tag{5}$$

The ξ parameter of each channel is calculated using the first and second moments of the considered channel, m_1 and m_2, as follows:

$$\xi_{sq} = \frac{m_1^2(n+1)}{n\,m_2 - m_1^2(n+1)}, \tag{6}$$

with $m_1 = \mathbb{E}(|S_{sq}|)$, and $m_2 = \mathbb{E}(|S_{sq}|^2)$, for $s, q = \{H, V\}$.

Analogously, the extremely heterogeneous areas model of the complex multi-look covariance matrix, obtained assuming $\xi < -1$, is [3]:

$$f_{(n)}(\boldsymbol{Z}) = \frac{n^{mn}|\boldsymbol{Z}|^{n-m}\Gamma(mn-\xi)}{h(n,m)|\boldsymbol{C}|^n\Gamma(-\xi)(-\xi-1)^n} \left(n\text{trace}\left(\boldsymbol{C}^{-1}\boldsymbol{Z}\right) + (-\xi-1)\right)^{\xi-mn}, \tag{7}$$

Notice that the multivariate distribution for the multi-look polarimetric covariance matrix, denoted $\mathcal{K}_P$, corresponds to (3). In contrast, (7) is denoted as $\mathcal{G}_P^0(\xi, \boldsymbol{C}, n)$. In the univariate case, [2] stated that $\mathcal{G}_I^0$ can be applied not only to extremely heterogeneous polarimetric clutter but also to describe both heterogeneous and homogeneous data. Similarly, [3] noted this for $\mathcal{G}_P^0$. Therefore, the proposal is to take advantage of this distribution in order to calculate an estimate of the covariance matrix, without making the assumption of homogeneity.

Furthermore, references [10]–[12] examined covariance matrix estimation challenges in heterogeneous environments for radar detection by proposing that elementary matrices extracted from training data maintain a consistent structure, albeit with varying scaling factors. Specifically, in [12], the authors introduced a class of estimators based on geometric medians of basic covariance matrices $\boldsymbol{Z}_i$, obtained from the available data set, and suitable distances in the considered space. More in detail, the covariance estimate is given by:

$$\hat{\boldsymbol{C}} = \arg\min_{\boldsymbol{C}} \left[\sum_{i=1}^{n} w_i d(\boldsymbol{Z}_i, \boldsymbol{C})\right], \tag{8}$$

where w_i, $w_i > 0$ and $\sum_{i=1}^{n} w_i = 1$, are the coefficients that weight the data according to their reliability, which is found solving a semi-definite programming (SDP) problem. Furthermore, in the context of the classification of polarimetric covariance symmetry, [13] implemented a pre-screening process on the SAR data, ensuring that the most homogeneous data were selected.

In this work, we propose to use the median matrix as described in [12], but considering the exploitation of an appropriate distance that explicitly attempts to account for

This article has been accepted for publication in IEEE Geoscience and Remote Sensing Letters. This is the author's version which has not been fully edited and content may change prior to final publication. Citation information: DOI 10.1109/LGRS.2025.3565808

heterogeneity in the data. In this respect, the multi-look polarimetric probability density function (pdf) of heterogeneous areas is utilized. Details of the proposed method are given in Section III.

III. Proposed method

To properly account for a heterogeneous environment, the $\mathcal{G}_P^0$ distribution is used in this work instead of the Wishart to model the polarimetric covariance matrix. In fact, some pixels in the window used to estimate the covariance matrix may contain targets with different covariance matrix structures. Therefore, to account for the heterogeneity of the data, the covariance matrix is estimated by calculating the geometric median in (8), with the distance given by the natural logarithm of the pdf in (7). Moreover, since it is not needed to weight the different elementary matrices, equal weights $w_i = 1/n$ are set into (8), namely:

$$\hat{\boldsymbol{C}} = \arg\min_{\boldsymbol{C}} \frac{1}{n}\sum_{i=1}^{n} d(\boldsymbol{Z}_i, \boldsymbol{C}), \tag{9}$$

or equivalently

$$\hat{\boldsymbol{C}} = \arg\min_{\boldsymbol{C}} \left[\sum_{i=1}^{n} \log(f_{(n)}(\boldsymbol{Z}_i, \boldsymbol{C}))\right]. \tag{10}$$

Substituting into (10) the expression of the pdf provided by (7), it becomes:

$$\begin{aligned}\hat{\boldsymbol{C}} = \arg\min_{\boldsymbol{C}} \Bigg[\sum_{i=1}^{n} &[(n-m)\log|\boldsymbol{Z}_i| - n\log|\boldsymbol{C}| + \\ &(\xi - nm)\log\left(n\,\mathrm{trace}\left(\boldsymbol{C}^{-1}\boldsymbol{Z}_i\right) + (-\xi - 1)\right)]\Bigg].\end{aligned} \tag{11}$$

Since $\boldsymbol{Z}_i$, $i = 1, \ldots, n$, is independent of $\boldsymbol{C}$ the optimization problem with respect to $\boldsymbol{C}$ is equivalent to the following:

$$\begin{aligned}\hat{\boldsymbol{C}} = \arg\min_{\boldsymbol{C}} \Bigg[&- n^2\log|\boldsymbol{C}| + \\ &(\xi - nm)\sum_{i=1}^{n}\log\left[n\,\mathrm{trace}\left(\boldsymbol{C}^{-1}\boldsymbol{Z}_i\right) + (-\xi - 1)\right]\Bigg].\end{aligned} \tag{12}$$

Hence, the median matrix is obtained as the matrix $\boldsymbol{C}$ that minimizes (12). However, since a closed-form solution to the above optimization problem is not available, it can be derived setting to zero its derivative and solving for the matrix argument. To this aim, let us proceed further with the calculation of the derivative of (12) with respect to $\boldsymbol{C}$.

Before proceeding further, let us recall some useful properties related to matrix derivatives. Let $\boldsymbol{X}$ be a complex matrix of size $n \times n$. Thus, the derivative of $\log|\boldsymbol{C}|$ with respect to the complex matrix $\boldsymbol{C}$ is (see [14, eq.57]):

$$\frac{d}{d\boldsymbol{C}}\log|\boldsymbol{C}| = \boldsymbol{C}^{-T}. \tag{13}$$

Let now proceed to the derivative of the following function involved in the summation of (12):

$$f(C) = \log\left(n\,\mathrm{trace}\left(C^{-1}\boldsymbol{Z}_i\right) + b\right). \tag{14}$$

Recalling that the derivative of $\log(x)$ with respect to x is $1/x$, we first differentiate the outer logarithmic function:

$$\begin{aligned}\frac{d}{d\boldsymbol{C}}f(\boldsymbol{C}) &= \frac{1}{n\,\mathrm{tr}(\boldsymbol{C}^{-1}\boldsymbol{Z}_i) + b}\cdot\frac{d}{d\boldsymbol{C}}\left(n\,\mathrm{tr}(\boldsymbol{C}^{-1}\boldsymbol{Z}_i) + b\right) \\ &= \frac{n}{n\,\mathrm{tr}(\boldsymbol{C}^{-1}\boldsymbol{Z}_i) + b}\cdot\frac{d}{d\boldsymbol{C}}\mathrm{tr}(\boldsymbol{C}^{-1}\boldsymbol{Z}_i).\end{aligned} \tag{15}$$

The derivative of the trace term (see [14, eq.63]) is:

$$\frac{d}{d\boldsymbol{C}}\mathrm{tr}(\boldsymbol{A}\boldsymbol{C}^{-1}\boldsymbol{Z}_i) = -\boldsymbol{C}^{-T}\boldsymbol{A}^T\boldsymbol{Z}_i^T\boldsymbol{C}^{-T}. \tag{16}$$

Thus, for $\boldsymbol{A}$ equal to the identity matrix $\mathbf{I}_d$, the latter equation becomes:

$$\frac{d}{d\boldsymbol{C}}f(\boldsymbol{C}) = \frac{-n\boldsymbol{C}^{-T}\boldsymbol{Z}_i^T\boldsymbol{C}^{-T}}{n\,\mathrm{tr}(\boldsymbol{C}^{-1}\boldsymbol{Z}_i) + b}. \tag{17}$$

Finally, from (13) and (17), and setting b to $-\xi - 1$, the considered optimization problem is effectively simplified to solving the following equation:

$$\sum_{i=1}^{n}\left[\frac{-(\xi - nm)\boldsymbol{C}^{-T}\boldsymbol{Z}_i^T\boldsymbol{C}^{-T}}{n\,\mathrm{tr}(\boldsymbol{C}^{-1}\boldsymbol{Z}_i) + (-\xi - 1)} - \boldsymbol{C}^{-T}\right] = \mathbf{0}. \tag{18}$$

The nonlinear equation (18) can be solved using a combination of the Powell and Newton methods [15]. This strategy benefits from the rapid convergence of the Newton method while ensuring reliability across various functions. The Powell method adds robustness in cases where Newton may struggle with poor initial guesses or function discontinuities. The SCM is used as an appropriate initial guess.

IV. Results and Discussions

The proposed approach has been tested using a fully-polarized dataset, acquired by the legacy Danish airborne SAR system EMISAR (developed by the former Electromagnetics Institute, now part of DTU Space), on April 17th 1998. The L-band SAR image covers a scene from the Foulum area in Denmark with a resolution of 2×2 m. An area of size 900×1000 pixels was selected due to its depiction of a diverse landscape that includes built-up areas, various types of vegetated fields, and few bodies of water, as illustrated in Figure 1. Moreover, the dataset comprised ground truth data consisting of aerial photographs along with information about land cover [16].

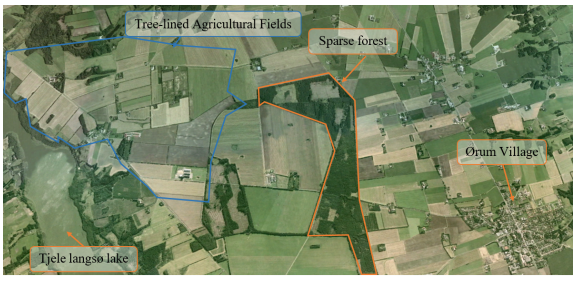

Figure 1: Google Earth© image of the studied zone.

Figure 2 shows the roughness parameter ξ, whose significance as a metric for quantifying surface roughness is

This article has been accepted for publication in IEEE Geoscience and Remote Sensing Letters. This is the author's version which has not been fully edited and content may change prior to final publication. Citation information: DOI 10.1109/LGRS.2025.3565808

evident. The figure provides a comprehensive representation of the variability in surface scattering characteristics. In particular, lower values of ξ indicate greater complexity and diversity in surface features, while higher values correspond to a more uniform surface. Regions with ξ values below 1 are characterized by relatively rough surfaces, indicative of high heterogeneity due to factors such as buildings, complex structures, dense vegetation, and water movement. Conversely, higher ξ values are associated with progressively smoother surfaces, typically found in more homogeneous areas with sparse vegetation or calm water. The predominance of low ξ values, as illustrated in Figure 2, supports the initial hypothesis that heterogeneity predominates in built-up areas and along the borders of agricultural lands. To highlight the advantages of the proposed technique over conventional methods, we calculated scattering entropy[1]. The resulting scattering entropy maps, derived from the eigenvalues of both methods, are shown in Figure 3.

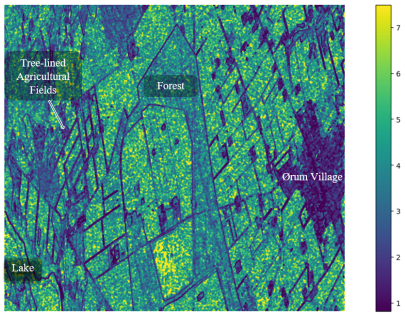

Figure 2: Roughness parameter ξ for the studied area of the L-band Foulum PolSAR data sized 900×1000 pixels.

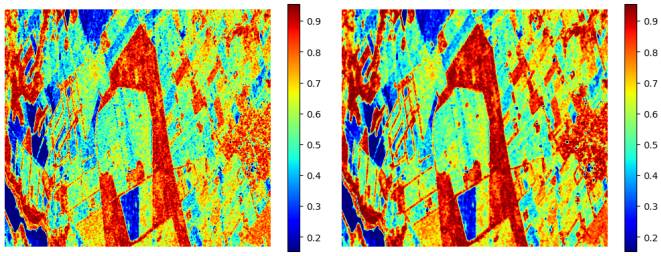

(a) (b)

Figure 3: Polarimetric entropy for the studied area calculated using (a) classical, and (b) proposed methods.

The findings illustrate on one hand a high density of pixels having an entropy value higher than 0.5, which suggests the presence of unpolarized scatterers (two or three scattering mechanisms taking place concurrently). Largely, high entropy indicates stronger heterogeneity or randomness in the scattering properties of the area, which concord again with the initial assumption. On the other hand, the refinement granted by the proposed algorithm can be observed in Figure 3(b) where the chaotic effect of different sub-areas disappeared.

[1]The entropy provides a general measure of scattering depolarization [1].

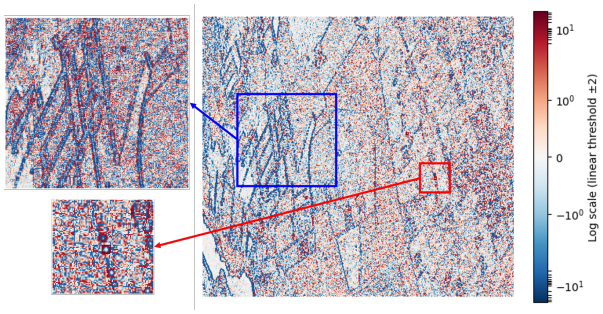

Figure 4: Mean alpha angle difference $\overline{\alpha}_{\text{median}} - \overline{\alpha}_{\text{SCM}}$.

This is due to the heterogeneity being considered by the $\mathcal{G}_P^0$ Wishart modeling of the covariance matrix.

To further assess the effectiveness of the proposed framework, the $\overline{\alpha}$ angle from the Cloude-Pottier decomposition [1] is also computed. This parameter characterizes the dominant scattering mechanism (such as surface, volume, or double-bounce scattering) and ranges from $0°$ to $90°$. To more clearly illustrate the contribution of the proposed method, the difference between the two $\overline{\alpha}$ angles, one estimated using the coherence matrix derived from the proposed approach and the other using the SCM is presented, namely $\overline{\alpha}_{\text{median}} - \overline{\alpha}_{\text{SCM}}$. A symmetrical logarithmic colour bar is employed as it effectively conveys both the sign (positive/negative) and magnitude (small/large) of the values. Values in the range of -2 to $+2$ are displayed linearly, while values lower than -2 are shown logarithmically in blue, and values higher than $+2$ are shown logarithmically in red. This representation preserves small variations, in contrast to a purely logarithmic scale, which would obscure low-magnitude values.

The results reveal that the $\overline{\alpha}$ values are noticeably higher in the proposed method (highlighted in dark red), particularly along the edges of tree lines and isolated buildings. This pattern suggests the presence of a double-bounce scattering mechanism rather than a volumetric one, an observation that will be corroborated by the classification presented in the following analysis. In addition, the appearance of dark blue regions indicates a decrease in the angle between the ground and tree lines. This leads to those pixels being classified as surface scattering instead of volumetric, resulting in a more refined delineation of the tree lines that more accurately reflects reality. An important advantage of this approach is that it does not assume homogeneity within the scene, thereby avoiding the overgeneralization that often leads to coarse pixel groupings.

To further demonstrate the improvements introduced by the proposed framework, the Freeman-Durden Wishart classification [17] is performed using both the traditional SCM and the proposed median matrix. This classification method is selected due to its robustness in accurately identifying a range of scattering mechanisms in PolSAR data. The classification results obtained from both the approaches are presented in Figure 5 for comparison.

A key observation when comparing the proposed method to SCM is its improved contour delineation. Isolated structures in the image center have borders and edges clearly distinguished

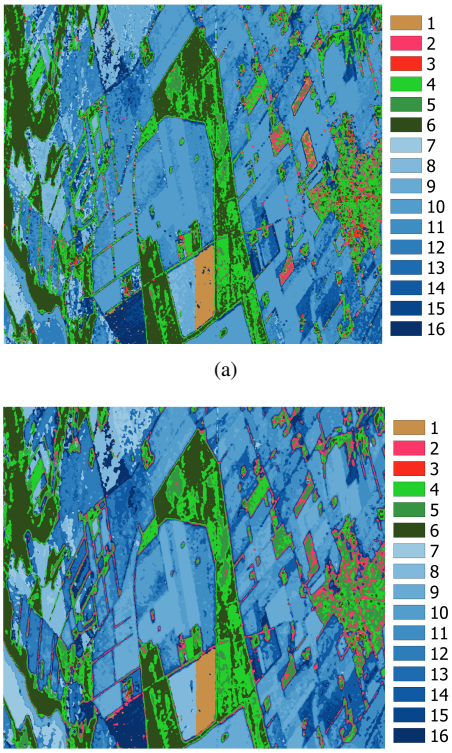

(a)

(b)

Figure 5: Freeman-Durden Wishart classification using (a) classical, and (b) proposed methods.

from interiors. The two main roads in Ørum village, lined with trees and buildings, are accurately detected as double-bounce areas, enhancing classification. This improvement arises because double-bounce occurs between the ground and buildings or tree trunks, whereas interiors are classified according to their surface or volume characteristics. Similarly, in the top-right of the image, small constructions and the main road in Mollerup village are also identified as double-bounce zones, contributing to greater accuracy. The primary advantage of this method is its detail preservation, due to the algorithm's lack of assumptions about homogeneity. This is evident in the well-defined tree lines in agricultural plots, as shown in Figure 5(b), where double-bounce returns from tree trunks and volume scattering from foliage are highlighted.

In contrast, the SCM homogenisation blends double-bounce and volume scattering, creating coarse clusters of pixels that blur details, as seen in Figure 5(a). While the tree lines are represented by a mixture of double bounce and volume classifications (classes 3, 4 and 6) in the SCM, the proposed method clearly identifies these plots and accurately reflects the tree lines with separate classifications for foliage as volume (classes 4 and 5) and double bounce (class 3) at the edges (trunk soil).

V. Conclusion

This paper presented an advanced method for covariance estimation specifically adapted to heterogeneous environments. The approach provided a more accurate representation of complex structures in highly rugged settings, where scattering mechanisms were not adequately captured by models that assumed homogeneity. The proposed method effectively preserved fine details, such as isolated objects, while ensuring accurate representation of features like roads and tree lines. The experimental results demonstrated that this methodology enhanced the segmentation and classification of polarimetric SAR images, maintaining sharp edges and clear details.

Acknowledgment

The authors would like to thank ESA for providing the EMISAR sample data, and the Technical University of Denmark (DTU) for ground truth data.

References

[1] J.-S. Lee and E. Pottier, *Polarimetric Radar Imaging: From Basics to Applications*. 2009.

[2] A. C. Frery, H.-J. Muller, C. d. C. F. Yanasse, and S. J. S. Sant'Anna, "A Model for Extremely Heterogeneous Clutter," *IEEE Transactions on Geoscience and Remote Sensing*, vol. 35, no. 3, pp. 648–659, 1997.

[3] C. C. Freitas, A. C. Frery, and A. H. Correia, "The Polarimetric G Distribution for SAR Data Analysis," *Environmetrics*, vol. 16, no. 1, pp. 13–31, 2005.

[4] M. M. Horta, N. D. Mascarenhas, and A. C. Frery, "A Comparison of Clustering Fully Polarimetric SAR Images using SEM Algorithm and $\mathcal{G}_P^0$ Mixture Model with Different Initializations," *Proceedings - International Conference on Pattern Recognition*, pp. 3–6, 2008.

[5] J. I. Fernández-Michelli, J. A. Areta, M. Hurtado, and C. H. Muravchik, "Polarimetric SAR Image Classification using EM Method and $\mathcal{G}_p^0$ Model," *2015 16th Workshop on Information Processing and Control*, 2016.

[6] Q. Xu, Q. Chen, S. Yang, and X. Liu, "Superpixel-Based Classification using K Distribution and Spatial Context for Polarimetric SAR Images," *Remote Sensing*, vol. 8, no. 8, 2016.

[7] G. C. Hu and Q. H. Zhao, "$\mathcal{G}_0$-Wishart Distribution Based Classification from Polarimetric SAR Images," *ISPRS Annals of the Photogrammetry, Remote Sensing and Spatial Information Sciences*, vol. 4, no. 2W4, pp. 451–455, 2017.

[8] C. Freitas, S. Sant'Anna, L. Soler, J. Santos, L. Dutra, L. de Araújo, J. Mura, and P. Hernandez Filho, "The Use of Airborne P-Band Radar Data for Land Use and Land Cover Mapping in Brazilian Amazonia," in *International Geoscience and Remote Sensing Symposium (IGARSS)*, vol. 4, pp. 1889–1891, IEEE, 2001.

[9] A. D. Nascimento, J. A. Ferreira, and A. C. Frery, "Unsupervised Segmentation of PolSAR Data with Complex Wishart and $\mathcal{G}_m^0$ Distributions and Shannon Entropy," *Statistics and Computing*, vol. 33, no. 129, 2023.

[10] A. Aubry, A. De Maio, L. Pallotta, and A. Farina, "Covariance Matrix Estimation via Geometric Barycenters and its Application to Radar Training Data Selection," *IET Radar, Sonar & Navigation*, vol. 7, no. 6, pp. 600–614, 2013.

[11] A. Aubry, A. De Maio, L. Pallotta, A. Farina, and C. Fantacci, "Median Matrices and Geometric Barycenters for Training Data Selection," in *2013 14th International Radar Symposium (IRS)*, vol. 1, pp. 331–336, 2013.

[12] A. Aubry, A. De Maio, L. Pallotta, and A. Farina, "Median Matrices and Their Application to Radar Training Data Selection," *IET Radar, Sonar & Navigation*, vol. 8, no. 4, pp. 265–274, 2014.

[13] L. Pallotta and M. Tesauro, "Outlier Rejection by Means of Median Matrices for Polarimetric SAR Covariance Symmetry Classification," *IEEE Geoscience and Remote Sensing Letters*, vol. 20, pp. 1–5, 2023.

[14] K. B. Petersen and M. S. Pedersen, "The matrix cookbook," 2012.

[15] M. Powell, "A Hybrid Method for Nonlinear Algebraic Equations," in *Numerical Methods for Nonlinear Algebraic Equations* (P. Rabinowitz, ed.), pp. 87–114, London, New York, Paris: Gordon and Breach, 1970.

[16] A. A. Nielsen, H. Skriver, and K. Conradsen, "Complex Wishart distribution based analysis of polarimetric synthetic aperture radar data," *Proceedings of MultiTemp 2007 - 2007 International Workshop on the Analysis of Multi-Temporal Remote Sensing Images*, 2007.

[17] J.-S. Lee, M. Grunes, E. Pottier, and L. Ferro-Famil, "Unsupervised Terrain Classification Preserving Polarimetric Scattering Characteristics," *IEEE Transactions on Geoscience and Remote Sensing*, vol. 42, no. 4, pp. 722–731, 2004.